Diverse Regional Sensitivity of Summer Precipitation in East Asia to Ice Volume, CO_2 and Astronomical Forcing

A. Lyu[1], Q. Yin[1]*, M. Crucifix[1], and Y. Sun[2,3]

[1]Georges Lemaître Center for Earth and Climate Research, Earth and Life Institute, Université Catholique de Louvain, 1348 Louvain-la-Neuve, Belgium.

[2]State Key Laboratory of Loess and Quaternary Geology, Institute of Earth Environment, Chinese Academy of Sciences, 710061 Xian, China.

[3]CAS Center for Excellence in Quaternary Science and Global Change, Chinese Academy of Sciences, 710061 Xian, China.

Corresponding author: Qiuzhen Yin (qiuzhen.yin@uclouvain.be)

Key Points:

- In northern East Asia, the variation of summer precipitation is dominated by precession.
- In southern East Asia, ice volume plays a more important role on the summer precipitation via its control on the location of ITCZ.
- The effects of obliquity and CO_2 on summer precipitation are very small compared to precession and ice volume.

Abstract

The relative influence of insolation, CO_2 and ice sheets on the East Asian summer monsoon (EASM) is not well understood especially at regional scale. Here a Gaussian emulator based on simulations with HadCM3 is used to quantitatively assess how astronomical forcing, CO_2 and northern hemisphere (NH) ice sheets affect the variation of the summer precipitation over the last 800 ky. Our results show that in the EASM domain north of 25°N, the variation of the summer precipitation is dominated by precession, leading to strong 23-ky cycles, while the ice sheets only modulate the effect of insolation by influencing the land-sea pressure gradient. In the southern part, ice sheets play a more important role, generating 100-ky cycles, through influencing the latitude of the Intertropical Convergence Zone (ITCZ) and the Hadley cell. Obliquity and CO_2 have little effect on the summer precipitation as compared to precession and ice sheets.

Plain Language Summary

The East Asian summer monsoon (EASM) is a wind which carries moist air from the Indian and Pacific Oceans to East Asia, and it affects the economy and life of a large population. On astronomical time scale, its variation is controlled by insolation, CO_2 and ice sheets. Here we use a Gaussian emulator based on climate simulations to assess how these factors affect the variation of the summer precipitation. In the northern part of the EASM domain, the summer precipitation has a strong 23-ky cycle. It is mainly controlled by precession. The effect of insolation is further modulated by ice sheets by the variations of the land-sea pressure gradient. In the southern part, ice sheets play a vital role on the summer precipitation via its control on the location of the Intertropical Convergence Zone (ITCZ). Obliquity and CO_2 have little effect on the precipitation.

1 Introduction

The East Asian summer monsoon (EASM) is an important component of the climate system and it influences the economy and life of a large population. Numerous paleoclimate records have been used to reconstruct the long-term evolution of the EASM (e.g., Guo et al. 2002; Wang et al., 2003; Sun et al., 2015, 2019; Wang, Y., et al., 2008; Clemens et al., 2010; Ao et al., 2011; Lu et al. 2013; Cheng et al., 2016). Climate simulations have also been used to explore the response of the EASM to different forcings (e.g., Wang, 1999; Yin et al., 2008, 2009; Shi et al., 2012; Jiang et al., 2013; Jin et al., 2014; Zhang et al., 2018; Shi et al., 2020; Wang et al., 2020; Zhang et al., 2020).

Since Kutzbach (1981) proposed the important influence of precession on Asian monsoon, the influence of summer solar radiation on the EASM evolution on the astronomical scale has been confirmed by more and more studies. The EASM is found strong at times of high summer insolation, when the land-ocean thermal contrast at surface is large (e.g., Kutzbach et al., 2008; Yin et al., 2009). The variation of $\delta^{18}O$ of the speleothems in southern China shows dominant ~19-23-ky cycles, in phase with summer insolation at 65°N (e.g., Cheng et al., 2016), also indicating a major control of the EASM by precession. However, in northern China, the magnetic susceptibility of the loess record, which is considered as a proxy for the EASM (e.g., An et al., 1990), shows dominant 100-ky cycles, suggesting a close relationship between the EASM and the changes in global ice volume (Lu et al., 2004). High-resolution loess records from northwestern Chinese Loess Plateau and marine records from the marginal seas surrounding China present three major cycles, namely ~19-23 ky, 41 ky and 100 ky (Chen et al., 2003; Sun et al., 2006; Yi et al., 2012; An et al., 2015), suggesting the joint control of precession, obliquity and ice volume on the EASM. The diverse periodic rhythms of the EASM variations revealed by different proxies might be related on the one hand to their different paleoclimate representations, and on the other hand to the regional diversity of the East Asian climate response to different forcings.

The response of the EASM precipitation to astronomical forcing and ice volume is indeed complex. Modelling studies of Yin et al (2008, 2009) show that the effects of ice sheets on the EASM depend on their location and size, and also on the background insolation. Weber and Tuenter (2011) found that insolation plays a dominant role on the EASM, and ice sheets just modulate the magnitude of the EASM's response to insolation. Recently, comparison of loess proxy with model results shows that the sensitivity of the EASM to insolation decreases as the NH became more glaciated after the mid-Pleistocene transition (Sun et al., 2019).

The strong regional dependence of the EASM variation as recorded in various proxy records questions the relative role of ice sheets and insolation on the EASM precipitation in different sub-regions in East Asia. In this study, we aim to investigate the relative importance of the astronomical forcing, ice sheets and CO_2 on the summer precipitation in different latitudes of the EASM domain over the last 800 ky. Sensitivity analysis of HadCM3 simulations using a Gaussian-process emulator are performed to quantitatively assess the role of different factors.

2 Methods and experiments setting

An emulator is a statistical model which is originated from a limited number of model runs covering a multidimensional input space (O'Hagan, 2006; Petropoulos et al., 2009). It provides an efficient and relatively low-cost method to visualize the effects of changing one single or a couple of parameters (Petropoulos et al., 2009). A detailed description of the Gaussian process emulator used here can be found in Araya-Melo et al. (2015) and Lord et al. (2017). It was generated and calibrated by interpolating the outputs of 61 snapshot simulations performed with the model HadCM3, following an experiment plan designed to optimize the emulator performance. The atmospheric component in HadCM3 has 19 layers in the vertical with a 2.5°×3.75° horizontal resolution. The spatial resolution over the ocean is 1.25°×1.25° with 20 vertical layers (Gordon et al., 2000). In the assessment of multi-model simulation on East Asia, HadCM3 shows good performances on different time scales (Jiang et al., 2005; Zhang et al., 2013). The snapshot experiments are 300-year long simulations and the last 50 years of the model runs are used for analyses. Using the emulator, we generate climate time series spanning the last 800 ky, forced with astronomical parameters (Berger and Loutre, 1991), CO_2 concentrations measured in the Antarctica ice core (Lüthi et al., 2008) and glaciation level, which was estimated by scaling the benthic $\delta^{18}O$ stack of the last 800 ky (Lisiecki & Raymo, 2005) from Level 1 to 11. Level 1 and 11 correspond to the present day and the Last Glacial Maximum, and level 2-10 stands for different amounts of ice volume. This method has been used to simulate the variations of Indian and East Asia summer monsoon during the Pleistocene (Araya-Melo et al., 2015; Sun et al., 2019).

Many studies show that the spatial variability of the summer precipitation in East Asia at present-day and in the last 500 years is characterized by a dipolar or tripolar mode pattern (e.g., Shi et al., 2019). Due to the strong regional dependence of the EASM (Wang, B., et al. 2008), in this study the East Asia (15°N-40°N and 105°E-120°E) is divided into five sub-regions every 5 degree along the meridian. Four groups of results are obtained by using only orbital forcing

(Orb), orbital with CO_2 forcing ($OrbCO_2$), orbital with ice sheet forcing (OrbIce) and orbital, CO_2 with ice sheet forcing ($OrbCO_2Ice$) as input, respectively. The performance of the emulator is evaluated by a leave-one-out cross-validation approach. The output of one experiment was compared with results predicted by an emulator based on the other 60 experiments left out (Fig. S1). The emulator can predict most of the outputs within one standard deviation when they are left out of the calibration procedure. To understand better the climate mechanisms, two additional experiments were performed with HadCM3 and compared with two experiments chosen from the 61 HadCM3 simulations used to calibrate the emulator. The experiment setting, including astronomical parameters, CO_2 concentrations and ice sheet is given in Table S1.

3 Results

3.1 Sensitivity of summer precipitation to astronomical forcing, CO_2 and ice sheet in different sub-regions

Abundant precipitation is brought over East Asia in summer by warm and moist EASM. Here we focus on precipitation in June, July and August (JJA) as precipitation is usually recorded in paleoclimate records to indicate the EASM intensity. Precipitation in other seasons is also analyzed by only briefly mentioned. Wavelet spectrum analysis is conducted to study the periodicity of the emulated JJA precipitation in each sub-region. The continuous wavelet transforms are performed using the MATLAB codes and a Morlet software package (Mallat, 1998; Torrence and Compo, 1998; Melice and Servain, 2003).

The summer precipitations emulated from Orb and from $OrbCO_2$ for the last 800 ky are displayed in Fig. 1a, with ice sheets being fixed at pre-industrial (PI) condition. The precipitation in the Orb group presents a consistent tendency with precession dominating in all latitudes. Spectral analysis also shows a clear 23-ky period corresponding to the main periodicity of precession (Fig. 1b). The important role of precession has been confirmed by many simulations with idealized astronomical forcing (e.g., Bosmans et al., 2018). It controls the seasonality of insolation at all latitudes and the summer precipitation is enhanced over Asia during minimum precession when summer insolation in the NH is increased. A relatively weak ~41-ky cycle brought by obliquity can be seen in the precipitation in 15-20°N. The effect of obliquity on tropical climate via a direct response to changes in the cross-equatorial insolation gradient has been demonstrated in other studies (e.g. Bosmans et al., 2015). In contrast, there are only some subtle differences between the precipitation in the Orb and $OrbCO_2$, implying that CO_2 has only but a relatively weak effect on precipitation. As the wavelet spectrum shows, the period of precipitation in the $OrbCO_2$ is also 23-ky, same as that in the Orb group (Fig. 1b).

Different from the Orb and $OrbCO_2$ groups, the periodicities of the summer precipitation variation in OrbIce and $OrbCO_2Ice$ depend strongly on latitudes. In general, the signals of the 41-ky band in all latitudes in OrbIce and $OrbCO_2Ice$ are stronger than those in Orb and $OrbCO_2$, which certainly reflects the influence of ice volume where strong 41-ky cycles can be found. In both OrbIce and $OrbCO_2Ice$, the precipitation variation to the north of 30°N have similar periodicity and magnitude as the one caused by orbital forcing alone, indicating the dominant role of insolation. In 25°-30°N, ice volume mainly affects the amplitude, but does not change the period of the summer precipitation. The JJA precipitation is significantly reduced in most periods of the last 800 ky except near the peaks of warm interglacials MIS-5e and MIS-11, when the benthic-$\delta^{18}O$ based ice volume reconstruction indicates an ice-level similar to today. However, the precipitation variation is still dominated by the 23-ky precession cycle (Fig.1). The largest impact of ice volume on summer precipitation occurs south of 25°N, with significant changes in both magnitude and periodicity of precipitation variation when compared to the impact of orbital forcing alone. In 20°-25°N, summer precipitation is mainly driven by ice volume, leading to a major periodicity of 100- ky, although precession and obliquity cycles are also visible. In 15°-20°N, the impact of ice volume is still strong, but its importance relative to precession is reduced as compared to 20°-25°N, leading to both strong 23-ky and 100-ky cycles in the precipitation variation. The response of the JJA precipitation to precession is advanced by about 3 ky in OrbIce and $OrbCO_2Ice$ as compared to Orb and $OrbCO_2$, leading to a phase difference between the two groups of simulations. This could be related to the nonlinear response of the EASM to different combinations of precession and ice volume as demonstrated in Yin et al (2009).

A variance-based analysis is conducted to quantify the impact of each forcing factor. To compute the sensitivity index of one parameter, we fix it at its actual value, compute the precipitation variance obtained by varying the other parameters throughout the 800 ky, and average this variance over the different values of the aimed parameter to obtain a mean variance. The total sensitivity index is defined as the mean variance divided by the full variance. The underlying theory and definitions are found in e.g., Saltelli (2004), and efficient computational approaches with emulator, accounting for the uncertainty introduced by the emulator are given in Oakley and O'Hagan (2004) and implemented in Araya-Melo et al. (2015). Figure 2 shows that the summer precipitation between 15°-40°N shows a weak sensitivity to CO_2 compared with other factors. As already discussed above, in the north of 25°N, the precipitation variation is most sensitive to precession, while ice volume and obliquity play a negligible role. In 20°-25°N, the sensitivity of precipitation variation to precession is smaller than that to ice volume. In 15°-20°N, precipitation change is sensitive to both precession and ice volume with precession being slightly more influent.

In summary, our model results show the relative importance of insolation and ice volume on the summer precipitation varies between regions. A strong precessional signal exists in the long-term variation of the summer precipitation in all latitudes, while precipitation shows a different degree of response to ice volume between the northern and southern part of the EASM domain, with the impact of ice volume more visible south of 30°N than in the north. The spatial difference in the summer precipitation response to precession and ice volume could at least partly explain some of the variations in the spectral signature observed in different proxies. For example, the stalagmite $\delta^{18}O$ record from Sanbao Cave (~31°N) (Wang, Y., et al., 2008), a pollen record from Lake Biwa in Japan (~35°N) (Nakagawa et al., 2008) and a bore core from Bohai (~37°N) (Yi et al., 2012) suggest a dominant effect of insolation and precession, while both ice volume and insolation changes appear to influence precipitation in South China Sea (~12°N) (Chen et al., 2003). In our study the 100-ky periodic signal in JJA precipitation in northern China is not as dominant as in the magnetic susceptibility of the loess records usually used an indicator of the EASM. However, the magnetic susceptibility of the loess is influenced not only by summer precipitation, but also by temperature and dust input (e.g., Han et al., 1996; Porter et al., 2001; Hao and Guo, 2005). Sun et al (2019, their Fig. 6) shows the annual mean temperature in 30°-40°N in East Asia has strong 100-ky periodicity due to the impact of ice volume. Therefore, the 100-ky periodicity in the magnetic susceptibility of the loess could results at least partly from the impact of temperature.

Unlike in northern China where summer precipitation dominates the annual precipitation, in southern China in particular south of 30°N, the precipitation in other seasons is not much less than the precipitation in summer. According to GPCC reanalysis data (1891-2016) (Schneider et al., 2011), JJA precipitation in 20°-25°N, 25°-30°N, 30°-35°N and 35°-40°N accounted for 47.5%, 38.2%, 48.9% and 61.0% of the year, respectively (There is almost no data in 15°-20°N because of the large area of ocean). Therefore, we have analyzed also the response of precipitation in other seasons and the whole year. Our results show that the response of precipitation in other individual seasons to insolation and ice volume is similar to what we have found for the summer precipitation in each sub-region. Annual mean precipitation contains more power at 100-ky and 40-ky cycles, and less power around 23-ky, compared to the seasonal precipitation, especially in northern China (Fig. S2). Our analysis shows that the effects of precession on precipitation in local winter and summer are opposite, so the signals of precession cancel each other on the annual scale. By contrast, the influence of ice sheet on precipitation in each season is similar so that its influence appears stronger in the annual mean. Therefore, a paleoclimate proxy for precipitation in northern China would exhibit 23-ky, 40-ky and 100-ky cycles if it is sensitive to annual precipitation changes, rather than only to changes in summer precipitation.

3.2 Mechanisms of diverse latitudinal response of summer precipitation to ice volume

To investigate the mechanisms causing latitudinal contrast in the response of the summer precipitation to ice volume, we analyze four additional HadCM3 experiments (Table S1). H insoLice and HinsoHice have similar latitudinal and seasonal distribution of insolation (Fig. S3) and CO_2 concentration, with boreal summer close to perihelion. The difference between them is mainly ice sheets, with much larger NH ice sheets in HinsoHice (Fig. S4). Their results reflect the impact of ice sheets under high summer insolation condition. LinsoLice and LinsoHice (Fig.S2) also have almost identical insolation and CO_2, and boreal summer occurs close to aphelion. The difference between them allows to identify the effect of ice sheets under low summer insolation condition.

The difference between HinsoHice and HinsoLice shows that large NH ice sheets lead to significant precipitation decrease in the EASM and the Indian monsoon domains, and the magnitude depends on regions (Fig. 3a & b). Precipitation decreases more in the south than in the north, and the maximum occurs between 15°N and 25°N. In contrast, the precipitation increases south of 10°N. The impact of ice sheet under low summer insolation has a similar pattern but with smaller magnitude of precipitation change (LinsoHice minus LinsoLice) in particular in the southern part. This shows that the impact of ice sheets on the EASM depends on the background insolation. Further analyses (Fig. S5) using more glaciation levels and more astronomical configurations show that the variations of summer precipitation induced by glaciation level depend on the background astronomical configuration, and those induced by a given astronomical configuration depend on glaciation levels, a result which is in line with the finding of Yin et al (2009) for MIS-13 using the LOVECLIM model. Fig. S5 shows that the relationship between precipitation and glaciation level is nonlinear in all the latitudinal bands except in 30°-35°N where a linear relationship is found. This nonlinear relationship is particularly pronounced in low latitudes 15°-20°N and 20°-25°N, which is probably related to strong internal feedbacks due to oceanic influence on the monsoon precipitation in low-latitudes such as for the Indian summer monsoon shown in Clemens et al (2008). Moreover, the relationship between precipitation and glaciation level varies for different astronomical configurations (Fig. S5), showing the necessity of taking into account the background astronomical forcing when discussing the effect of ice sheets on the EASM.

The controlling factors of EASM precipitation include the land–sea pressure gradient, atmosphere moisture content, and the location of the Intertropical Convergence Zone (ITCZ). Thus, the related processes are further analyzed.

First, the precipitation variation in Northern China is investigated. It is generally admitted that the large-scale surface cooling induced by ice sheets reduces the land-ocean pressure gradient contrast and weakens the EASM circulation. For example, in response to the forcing under the Last Glacial Maximum (LGM) conditions, the annual precipitation decreased by 7–29% averaged over China compared with the pre-industrial period in different models (Tian and Jiang, 2016). Ice sheets cause a low pressure anomaly over northern Pacific and a high pressure anomaly over the Eurasian continent, leading to a reduced land-sea pressure gradient, generating anomalous northwesterly winds over East China (Fig. 3c). These changes are consistent with the effect of the LGM ice sheet as simulated in the model NESM v1, which has a similar resolution as HadCM3 (Cao et al., 2019). Reduced land-sea pressure contrasts lead to a weakening of the EASM. Accordingly, the water vapor flux from the Northwest Pacific, one of the major moisture sources for the EASM precipitation, is also reduced (Fig. 3d). Low insolation causes similar anomalous patterns in pressure, winds and temperature, but the magnitude of changes is smaller than in the high insolation condition (not shown).

The change in pressure gradient could explain the inland drought over China, but cannot explain the maximum drought centered in ~20°N in Southern China. The location of the monsoon precipitation belt and the EASM precipitation intensity are also strongly associated with the location of the ITCZ (Chen et al., 2004; Lu et al., 2013; Ding et al., 2018). The ITCZ responses to the differential heating between the two hemispheres, and the transport of moisture and energy caused by the Hadley Cell partially compensates for the imbalance between the two hemispheres (Kang et al., 2008; Schneider et al. 2014; Byrne et al., 2018). In the LGM simulations (hence, NH cooling), the NH ice sheets shift the ITCZ southwards (Broccoli et al., 2006; Braconnot et al., 2007). One way to quantify the movement of ITCZ is to identify the latitude closest to the equator where the annual mean streamfunction (vertically averaged with mass weighting between 700 and 300 hPa) is zero, as done in Byrne et al. (2018). Using this method, our results show that the location of the ITCZ is very sensitive to ice volume, and it is shifted significantly to the south under large ice sheets condition (Fig. S6). However, compared to ice volume, the impact of insolation on the location of ITCZ is relatively small.

Figure 4 shows the JJA vertical velocity anomalies (positive vertical velocity indicated by negative omega) in pressure coordinates over 105°-120°E. In HinsoLice, the maximum rising center of the JJA vertical velocity --- the ascending branch of the Hadley Cell --- is at ~19°N (Fig. 4a). Compared to HinsoLice, in HinsoHice there is a subsidence anomaly north of ~12°N and centered around ~20°N, and an ascending anomaly at ~10°N (Fig. 4b, HinsoHice minus HinsoLice). This clearly indicates a southward shift of the ITCZ in response to the ice sheet. Fig. 4b also shows that the impact of the change in ITCZ is mainly over southern China (south of 25°N), which explains the stronger drought in southern China than in northern China in response to the ice sheet forcing (Fig. 3a). The decreasing precipitation in India, Tibet Plateau, West Africa and Tropic Pacific confirms the southward shift of ITCZ. Under low insolation condition, ice sheets also lead to a southward shift of ITCZ (Fig. 4b, LinsoHice minus LinsoLice) but to a lesser degree compared to what is found under high insolation condition. Hence, precipitation in southern China is also less affected by ice sheets in low insolation condition (Fig. 3b).

In summary, as the vertical convergence/divergence of the moisture change is under the control of the ITCZ, the convection precipitation in the south of the EASM domain is influenced to a larger extent by ITCZ than in the north. Precipitation in the south of 25°N is more sensitive to the glaciation level, which influences the precipitation there through its control on the location of ITCZ.

4 Conclusions

Insolation and ice sheets are both important factors controlling the East Asian summer monsoon precipitation. Our study shows that in the north of 25°N of the EASM domain, the variation of the summer precipitation is dominated by precession, and ice volume only modulates the effect of insolation through influencing the land-sea pressure contrast. This leads to strong 23-ky cycles in the summer precipitation. However, in the southern part (south of 25°N), the impact of ice volume becomes more important, leading to strong 100-ky cycles. Ice volume controls the precipitation in the southern part via its dominant control on the location of the ITCZ. The region under control of the ITCZ is more sensitive to the influence of ice volume than other regions. The effect of ice volume on summer precipitation depends on background astronomical configurations and vice versa. The relationship between summer precipitation and glaciation level varies among latitudes and for different astronomical configurations. Our results also show that obliquity and CO_2 have a small effect on the summer precipitation compared to the influence of precession and ice sheets.

Acknowledgments, Samples, and Data

This work is supported by the Fonds de la Recherche Scientifique-FNRS (F.R.S.-FNRS) under grant MIS F.4529.18. A. Lyu is supported by China Scholarship Council (CSC) Grant #201706190226. Q. Yin is Research Associate of F.R.S.-FNRS. Computational resources have been provided by the supercomputing facilities of the Université catholique de Louvain (CISM/UCL) and the Consortium des Équipements de Calcul Intensif en Fédération Wallonie Bruxelles (CÉCI) funded by the Fond de la Recherche Scientifique de Belgique (F.R.S.-FNRS) under convention 2.5020.11. We thank the two anonymous reviewers for their constructive comments.

Data availability statement: The data used in this study can be downloaded from the link https://zenodo.org/record/4581647.

References

An, Z. S., Liu, T. S., Lu, Y. C., Porter, S. C., Kukla, G., Wu, X. H., & Hua, Y. M. (1990). The long-term paleomonsoon variation recorded by the loess-paleosol sequence in central China. *Quaternary International*, *7*, 91-95. doi:10.1016/1040-6182(90)90042-3

An, Z. S., Wu, G. X., Li, J. P., Sun, Y. B., Liu, Y. M., Zhou, W. J., et al. (2015). Global monsoon dynamics and climate change. *Annual Review of Earth and Planetary Sciences*, 43, 29-77. doi:10.1146/annurev-earth-060313-054623

Ao, H., Dekkers, M. J., Qin, L., & Xiao, G. (2011). An updated astronomical timescale for the Plio-Pleistocene deposits from South China Sea and new insights into Asian monsoon evolution. *Quaternary Science Reviews*, 30(13-14), 1560-1575. doi:10.1016/j.quascirev.2011.04.009

Araya-Melo, P. A., Crucifix, M., & Bounceur, N. (2015). Global sensitivity analysis of the Indian monsoon during the Pleistocene. *Climate of the Past*, 11(1), 45-61. doi:10.5194/cp-11-452015

Berger, A., & Loutre, M. F. (1991). Insolation values for the climate of the last 10 million years. *Quaternary Science Reviews*, 10(4), 297-317. doi:10.1016/0277-3791(91)90033-Q

Bosmans, J. H. C., Hilgen, F. J., Tuenter, E., & Lourens, L. J. (2015). Obliquity forcing of low-latitude climate. *Climate of the Past*, 11(10), 1335-1346. doi:10.5194/cp-11-1335-2015

Bosmans, J. H. C., Erb, M. P., Dolan, A. M., Drijfhout, S. S., Tuenter, E., Hilgen, F. J., et al. (2018). Response of the Asian summer monsoons to idealized precession and obliquity forcing in a set of GCMs. *Quaternary Science Reviews*, 188, 121-135. doi:10.1016/j.quascirev.2018.03.025

Braconnot, P., Otto-Bliesner, B., Harrison, S., Joussaume, S., Peterchmitt, J. Y., Abe-Ouchi, A., et al. (2007). Results of PMIP2 coupled simulations of the Mid-Holocene and Last Glacial Maximum–Part 2: feedbacks with emphasis on the location of the ITCZ and mid-and high latitudes heat budget. *Climate of the Past*, 3 (2), 279-296. doi:10.5194/cp-3-279-2007

Broccoli, A. J., Dahl, K. A., & Stouffer, R. J. (2006). Response of the ITCZ to Northern Hemisphere cooling. *Geophysical Research Letters*, 33(1). doi:10.1029/2005GL024546

Byrne, M. P., Pendergrass, A. G., Rapp, A. D., & Wodzicki, K. R. (2018). Response of the intertropical convergence zone to climate change: Location, width, and strength. *Current Climate Change Reports*, 4(4), 355-370. doi:10.1007/s40641-018-0110-5

Cao, J., Wang, B., & Liu, J. (2019). Attribution of the Last Glacial Maximum climate formation. *Climate Dynamics*, 53(3-4), 1661-1679. doi:10.1007/s00382-019-04711-6

Chen, M. T., Shiau, L. J., Yu, P. S., Chiu, T. C., Chen, Y. G., & Wei, K. Y. (2003). 500 000Year records of carbonate, organic carbon, and foraminiferal sea-surface temperature from the southeastern South China Sea (near Palawan Island). *Palaeogeography, Palaeoclimatology, Palaeoecology*, 197(1-2), 113-131. doi:10.1016/S0031-0182(03)00389-4

Chen, T. C., Wang, S. Y., Huang, W. R., & Yen, M. C. (2004). Variation of the East Asian summer monsoon rainfall. *Journal of Climate*, 17(4), 744-762. doi:10.1175/15200442(2004)017<0744:VOTEAS>2.0.CO;2

Cheng, H., Edwards, R. L., Sinha, A., Spötl, C., Yi, L., Chen, S., et al. (2016). The Asian monsoon over the past 640,000 years and ice age terminations. *Nature*, 534(7609), 640-646. doi:10.1038/nature18591

Clemens, S. C., Prell, W. L., Sun, Y., Liu, Z., & Chen, G. (2008). Southern Hemisphere forcing of Pliocene $\delta^{18}O$ and the evolution of Indo-Asian monsoons. *Paleoceanography*, 23, PA4210. doi:10.1029/2008PA001638

Clemens, S. C., Prell, W. L., & Sun, Y. (2010). Orbital-scale timing and mechanisms driving Late Pleistocene Indo-Asian summer monsoons: Reinterpreting cave speleothem $\delta^{18}O$. *Paleoceanography*, 25, PA4207. doi:10.1029/2010PA001926.

Ding, Y., Si, D., Liu, Y., Wang, Z., Li, Y., Zhao, L., & Song, Y., 2018. On the characteristics, driving forces and inter-decadal variability of the East Asian summer monsoon. *Chinese Journal of Atmospheric Sciences (in Chinese),* 42 (3): 533-558. doi:10.3878/j.issn.10069895.1712.17261.

Gordon, C., Cooper, C., Senior, C. A., Banks, H., Gregory, J. M., Johns, T. C., et al. (2000). The simulation of SST, sea ice extents and ocean heat transports in a version of the Hadley Centre coupled model without flux adjustments. *Climate dynamics*, 16, 147-168. doi:10.1007/s003820050010

Guo, Z. T., Ruddiman, W. F., Hao, Q. Z., Wu, H. B., Qiao, Y. S., Zhu, R. X., et al. (2002). Onset of Asian desertification by 22 Myr ago inferred from loess deposits in China. *Nature*, 416, 159163. doi:10.1038/416159a

Han, J. M., Lu, H. Y., Wu, N. Q., & Guo, Z. T. (1996). The magnetic susceptibility of modern soils in China and its use for paleoclimate reconstruction. *Studia Geophysica et Geodaetica*, 40(3), 262-275. doi:10.1007/BF02300742

Hao, Q., & Guo, Z. (2005). Spatial variations of magnetic susceptibility of Chinese loess for the last 600 kyr: implications for monsoon evolution. *Journal of Geophysical Research: Solid Earth*, 110, B12101, doi:10.1029/2005JB003765.

Jiang, D., & Lang, X. (2010). Last glacial maximum East Asian monsoon: Results of PMIP simulations. *Journal of Climate*, 23(18), 5030-5038. doi:10.1175/2010JCLI3526.1

Jiang, D., Lang, X., Tian, Z., & Ju, L. (2013). Mid-Holocene East Asian summer monsoon strengthening: Insights from Paleoclimate Modeling Intercomparison Project (PMIP) simulations. *Palaeogeography, Palaeoclimatology, Palaeoecology*, 369, 422-429. doi:10.1016/j.palaeo.2012.11.007

Jiang, D.B., Wang, H. J., & Lang, X. M. (2005). Evaluation of East Asian climatology as simulated by seven coupled models. *Advances in Atmospheric Sciences*, 22(4), 479-495. doi:10.1007/BF02918482

Jin, L., Schneider, B., Park, W., Latif, M., Khon, V., & Zhang, X. (2014). The spatial–temporal patterns of Asian summer monsoon precipitation in response to Holocene insolation change: a model-data synthesis. *Quaternary Science Reviews*, 85, 47-62. doi:10.1016/j.quascirev.2013.11.004

Kang, S. M., Held, I. M., Frierson, D. M., & Zhao, M. (2008). The response of the ITCZ to extratropical thermal forcing: Idealized slab-ocean experiments with a GCM. *Journal of Climate*, 21(14), 3521-3532. doi:10.1175/2007JCLI2146.1

Kukla, G., An, Z. S., Melice, J. L., Gavin, J., & Xiao, J. L. (1990). Magnetic susceptibility record of Chinese loess. *Transactions of the Royal Society of Edinburgh: Earth Sciences*, 81(4), 263288.DOI: doi:10.1017/S0263593300020794

Kutzbach, J. E. (1981). Monsoon climate of the early Holocene: climate experiment with the earth's orbital parameters for 9000 years ago. *Science*, 214(4516), 59-61. doi:10.1126/science.214.4516.59

Kutzbach, J. E., Liu, X., Liu, Z., & Chen, G. (2008). Simulation of the evolutionary response of global summer monsoons to orbital forcing over the past 280,000 years. *Climate Dynamics*, 30(6), 567-579. doi:10.1007/s00382-007-0308-z

Lisiecki, L. E., & Raymo, M. E. (2005). A Pliocene-Pleistocene stack of 57 globally distributed benthic $\delta^{18}O$ records. *Paleoceanography*, 20, PA1003. doi:10.1029/2004PA001071

Lord, N. S., Crucifix, M., Lunt, D. J., Thorne, M. C., Bounceur, N., Dowsett, H., et al. (2017). Emulation of long-term changes in global climate: application to the late Pliocene and future. *Climate of the Past*, 13, 1539–1571. doi:10.5194/cp-13-1539-2017, 2017.

Lu, H., Yi, S., Liu, Z., Mason, J. A., Jiang, D., Cheng, J., et al. (2013). Variation of East Asian monsoon precipitation during the past 21 ky and potential CO_2 forcing. *Geology*, 41(9), 10231026. doi:10.1130/G34488.1

Lu, H., Zhang, F., Liu, X., & Duce, R. A. (2004). Periodicities of palaeoclimatic variations recorded by loess-paleosol sequences in China. *Quaternary Science Reviews*, 23(18-19), 18911900. doi:10.1016/j.quascirev.2004.06.005

Lüthi, D., Le Floch, M., Bereiter, B., Blunier, T., Barnola, J. M., Siegenthaler, U., et al. (2008). High-resolution carbon dioxide concentration record 650,000–800,000 years before present. *Nature*, 453(7193), 379-382. doi:10.1038/nature06949

Mallat, S. (1998). A wavelet tour of signal processing. Academic Press.

Mélice, J., & Servain, J. (2003). The tropical Atlantic meridional SST gradient index and its relationships with the SOI, NAO and Southern Ocean. *Climate Dynamics*, 20, 447-464. doi:10.1007/s00382-002-0289-x

Nakagawa, T., Okuda, M., Yonenobu, H., Miyoshi, N., Fujiki, T., Gotanda, K., et al. (2008). Regulation of the monsoon climate by two different orbital rhythms and forcing mechanisms. *Geology*, 36(6), 491-494. doi:10.1130/G24586A.1

O'Hagan, A. (2006). Bayesian analysis of computer code outputs: A tutorial. *Reliability Engineering & System Safety*, 91(10-11), 1290-1300. doi:10.1016/j.ress.2005.11.025

Oakley, J. E., & O'Hagan, A. (2004). Probabilistic sensitivity analysis of complex models: a Bayesian approach. *Journal of the Royal Statistical Society: Series B (Statistical Methodology)*, 66(3), 751-769. doi:10.1111/j.1467-9868.2004.05304.x

Petropoulos, G., Wooster, M. J., Carlson, T. N., Kennedy, M. C., & Scholze, M. (2009). A global Bayesian sensitivity analysis of the 1d SimSphere soil–vegetation–atmospheric transfer (SVAT) model using Gaussian model emulation. *Ecological Modelling*, 220(19), 2427-2440. doi:10.1016/j.ecolmodel.2009.06.006

Porter, S. C., Hallet, B., Wu, X., & An, Z. (2001). Dependence of near-surface magnetic susceptibility on dust accumulation rate and precipitation on the Chinese Loess Plateau. *Quaternary Research*, 55(3), 271-283. doi:10.1006/qres.2001.2224

Saltelli, A., Tarantola, S., Campolongo, F., & Ratto, M. (2004). Sensitivity analysis in practice: a guide to assessing scientific models (Vol. 1). New York: Wiley.

Schneider, T., Bischoff, T., & Haug, G. H. (2014). Migrations and dynamics of the intertropical convergence zone. *Nature*, 513, 45-53. doi:10.1038/nature13636

Schneider, U., Becker, A., Finger, P., Meyer-Christoffer, A., Rudolf, B., & Ziese, M. (2011). GPCC Full Data Reanalysis Version 6.0 at 0.5°: Monthly Land-Surface Precipitation from Rain-Gauges built on GTS-based and Historic Data. doi:10.5676/DWD_GPCC/FD_M_V7_050

Shi, F., Goosse, H., Klein, F., Zhao, S., Liu, T., & Guo, Z. (2019). Monopole mode of precipitation in East Asia modulated by the South China Sea over the last four centuries. *Geophysical Research Letters*, 46(24), 14713-14722. doi:10.1029/2019GL085320

Shi, F., Yin, Q., Nikolova, I., Berger, A., Ramstein, G., & Guo, Z. (2020). Impacts of extremely asymmetrical polar ice sheets on the East Asian summer monsoon during the MIS-13 interglacial. *Quaternary Science Reviews*, 230, 106164. doi:10.1016/j.quascirev.2020.106164

Shi, Z., Liu, X., & Cheng, X. (2012). Anti-phased response of northern and southern East Asian summer precipitation to ENSO modulation of orbital forcing. *Quaternary Science Reviews*, 40, 30-38. doi:10.1016/j.quascirev.2012.02.019

Sun, Y.B., Chen, J., Clemens, S.C., Liu, Q.S., Ji, J.F., & Tada, R. (2006). East Asian monsoon variability over the last seven glacial cycles recorded by a loess sequence from the northwestern Chinese Loess Plateau. *Geochemistry Geophysics Geosystems*, 7, Q12Q02. doi:10.1029/2006GC001287

Sun, Y.B., Kutzbach J., An Z.S., Clemens S, Liu Z.Y., Liu W.G., et al. (2015). Astronomical and glacial forcing of East Asian summer monsoon variability. *Quaternary Science Reviews* 115, 132-142. doi:10.1016/j.quascirev.2015.03.009

Sun, Y., Yin, Q., Crucifix, M., Clemens, S. C., Araya-Melo, P., Liu, W., et al. (2019). Diverse manifestations of the mid-Pleistocene climate transition. *Nature communications*, 10, 352. doi:10.1038/s41467-018-08257-9

Tian, Z., & Jiang, D. (2016). Revisiting last glacial maximum climate over China and East Asian monsoon using PMIP3 simulations. *Palaeogeography, Palaeoclimatology, Palaeoecology*, 453, 115-126. doi:10.1016/j.palaeo.2016.04.020

Torrence, C., & Compo, G. P. (1998). A practical guide to wavelet analysis. *Bulletin of the American Meteorological society*, 79(1), 61-78. doi:10.1175/1520-0477(1998)079<0061:APGTWA>2.0.CO;2

Wang, H. J. (1999). Role of vegetation and soil in the Holocene megathermal climate over China. *Journal of Geophysical Research: Atmospheres*, 104(D8), 9361-9367. doi:10.1029/1999JD900049

Wang, B., Wu, Z., Li, J., Liu, J., Chang, C. P., Ding, Y., & Wu, G. (2008). How to measure the strength of the East Asian summer monsoon. *Journal of Climate*, 21(17), 4449-4463. doi:10.1175/2008JCLI2183.1

Wang, N., Jiang, D., & Lang, X. (2020). Mechanisms for Spatially Inhomogeneous Changes in East Asian Summer Monsoon Precipitation during the Mid-Holocene. *Journal of Climate*, 33(8), 2945-2965. doi:10.1175/JCLI-D-19-0565.1

Wang, P. X., Wang, B., Cheng, H., Fasullo, J., Guo, Z., Kiefer, T., & Liu, Z. (2017). The global monsoon across time scales: Mechanisms and outstanding issues. *Earth-Science Reviews,* 174, 84-121. doi:10.1016/j.earscirev.2017.07.006

Wang, P., Jian, Z., Zhao, Q., Li, Q., Wang, R., Liu, Z., et al. (2003). Evolution of the South

China Sea and monsoon history revealed in deep-sea records. *Chinese Science Bulletin*, 48(23), 2549-2561. doi:10.1360/03wd0156

Wang, Y., Cheng, H., Edwards, R. L., Kong, X., Shao, X., Chen, S., et al. (2008). Millennial-and orbital-scale changes in the East Asian monsoon over the past 224,000 years. *Nature*, 451(7182), 1090-1093. doi:10.1038/nature06692

Weber, S. L., & Tuenter, E. (2011). The impact of varying ice sheets and greenhouse gases on the intensity and timing of boreal summer monsoons. *Quaternary Science Reviews*, 30(3-4), 469479. doi:10.1016/j.quascirev.2010.12.009

Yi, L., Yu, H. J., Ortiz, J. D., Xu, X. Y., Chen, S. L., Ge, J. Y., et al. (2012). Late Quaternary linkage of sedimentary records to three astronomical rhythms and the Asian monsoon, inferred from a coastal borehole in the south Bohai Sea, China. *Palaeogeography, Palaeoclimatology, Palaeoecology*, 329, 101-117. doi:10.1016/j.palaeo.2012.02.020

Yin, Q. Z., Berger, A., & Crucifix, M. (2009). Individual and combined effects of ice sheets and precession on MIS-13 climate. *Climate of the Past*, 5, 229–243. doi:10.5194/CP-5-229-2009

Yin, Q. Z., Berger, A., Driesschaert, E., Goosse, H., Loutre, M. F., & Crucifix, M. (2008). The Eurasian ice sheet reinforces the East Asian summer monsoon during the interglacial 500 000 years ago. *Climate of the Past*, 4, 79–90. doi:10.5194/cp-4-79-2008

Zhang, R., Yan, Q., Zhang, Z. S., Jiang, D., Otto-Bliesner, B. L., Haywood, A. M., et al. (2013). Mid-Pliocene East Asian monsoon climate simulated in the PlioMIP. *Climate of the Past*, 9, 2085-2099. doi:10.5194/cp-9-2085-2013

Zhang, X., Jin, L., Lu, H., Park, W., Schneider, B., & Latif, M. (2018). East–west contrast of Northeast Asian summer precipitation during the Holocene. *Global and Planetary Change*, 170, 190-200. doi:10.1016/j.gloplacha.2018.08.018

Zhang, Y., Renssen, H., Seppä, H., Valdes, P. J., & Li, J. (2020). Spatial contrasts of the Holocene hydroclimate trend between North and East Asia. *Quaternary Science Reviews*, 227, 106036. doi:10.1016/j.quascirev.2019.106036

Figure 1 (a) Emulated JJA precipitation for each latitude band. The black, green, blue and red lines stand for results calculated from Orb, OrbCO_2, OrbIce and OrbCO_2Ice, respectively. **(b)** Wavelet spectrum analysis for JJA precipitation. The first, second, third and fourth column stand for results calculated from Orb, OrbCO_2, OrbIce and OrbCO_2Ice, respectively.

Figure 2 The total sensitivity index of each variable.

Figure 3 JJA precipiation (mm/day) anomaly of **(a)** HinsoHice minus HinsoLice and **(b)** LinsoHice minus LinsoLice. **(c)** JJA geopotential (color shaded, gpm) and winds (arrow, m/s) on 850hPa anomaly (the regions below the topographic heights are set as missing values); **(d)** JJA vertically integrated water vapor transport flux anomaly (kg/ms) (Only differences exceeding the 95% confidence level are plotted) of Hinso-Hice minus Hinso-Lice.

Figure 4 (a) JJA vertical velocity (negative omega indicates rising motion and vice versa) in pressure coordinates integrated over 105°-120°E of four experiments; **(b)** JJA vertical velocity anomaly of HinsoHice minus HinsoLice and LinsoHice minus LinsoLice.

Figure 1

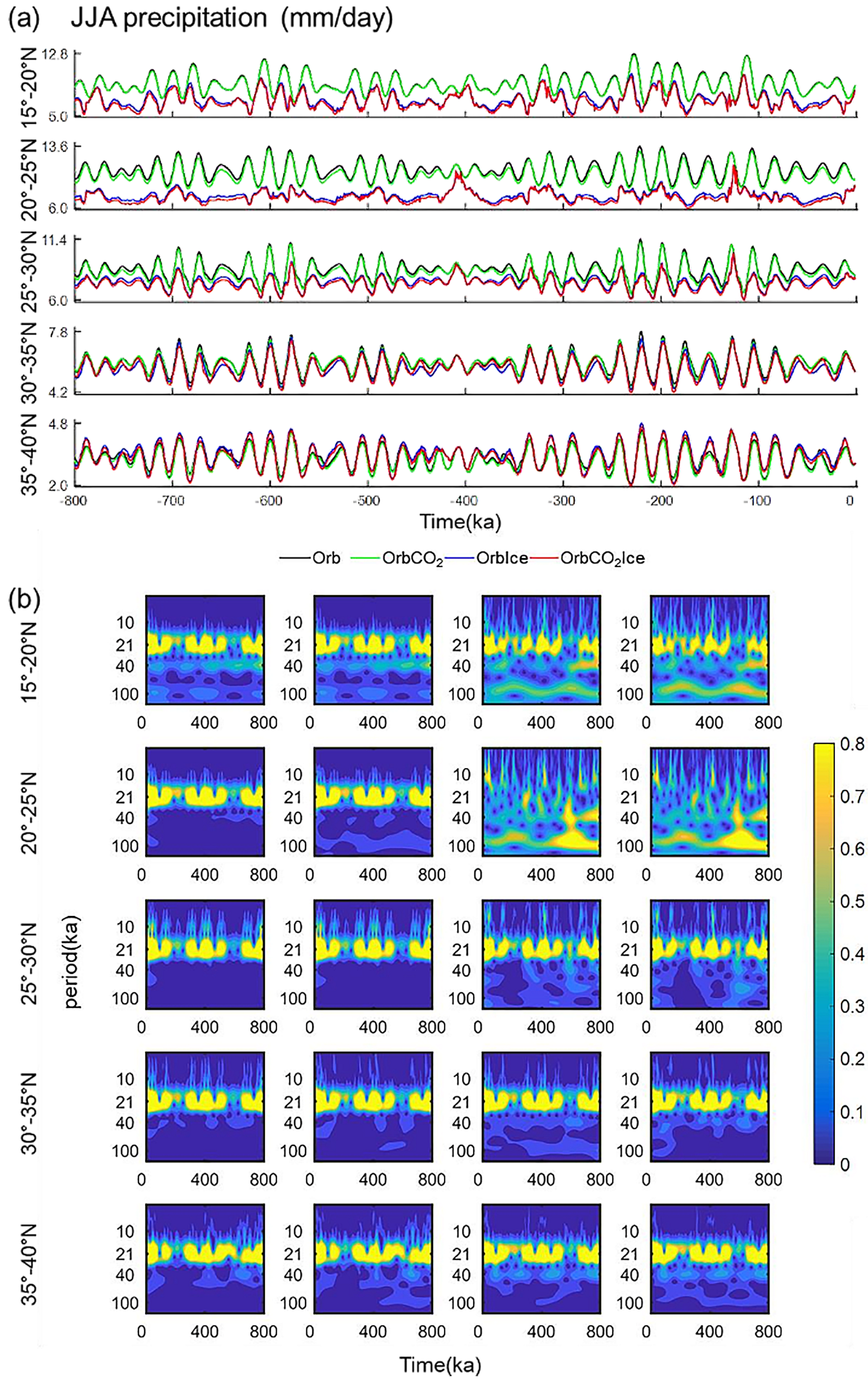
(a) JJA precipitation (mm/day)
15°-20°N
20°-25°N
25°-30°N
30°-35°N
35°-40°N
12.8
5.0
13.6
6.0
11.4
6.0
7.8
4.2
4.8
2.0
-800
-700
-600
-500
-400
-300
-200
-100
0
Time(ka)
Orb
OrbCO2
OrbIce
OrbCO2Ice
(b)
period(ka)
10
21
40
100
0
400
800
Time(ka)
0.8
0.7
0.6
0.5
0.4
0.3
0.2
0.1
0

Figure 2

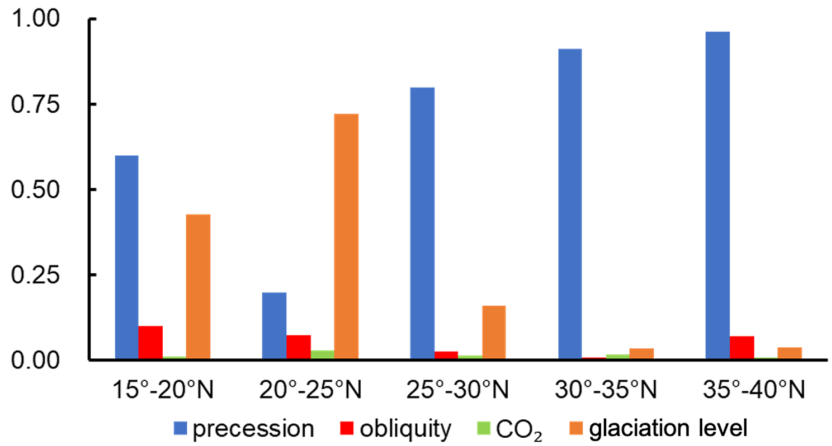
1.00
0.75
0.50
0.25
0.00
15°-20°N
20°-25°N
25°-30°N
30°-35°N
35°-40°N
precession
obliquity
CO_2
glaciation level

Figure 3

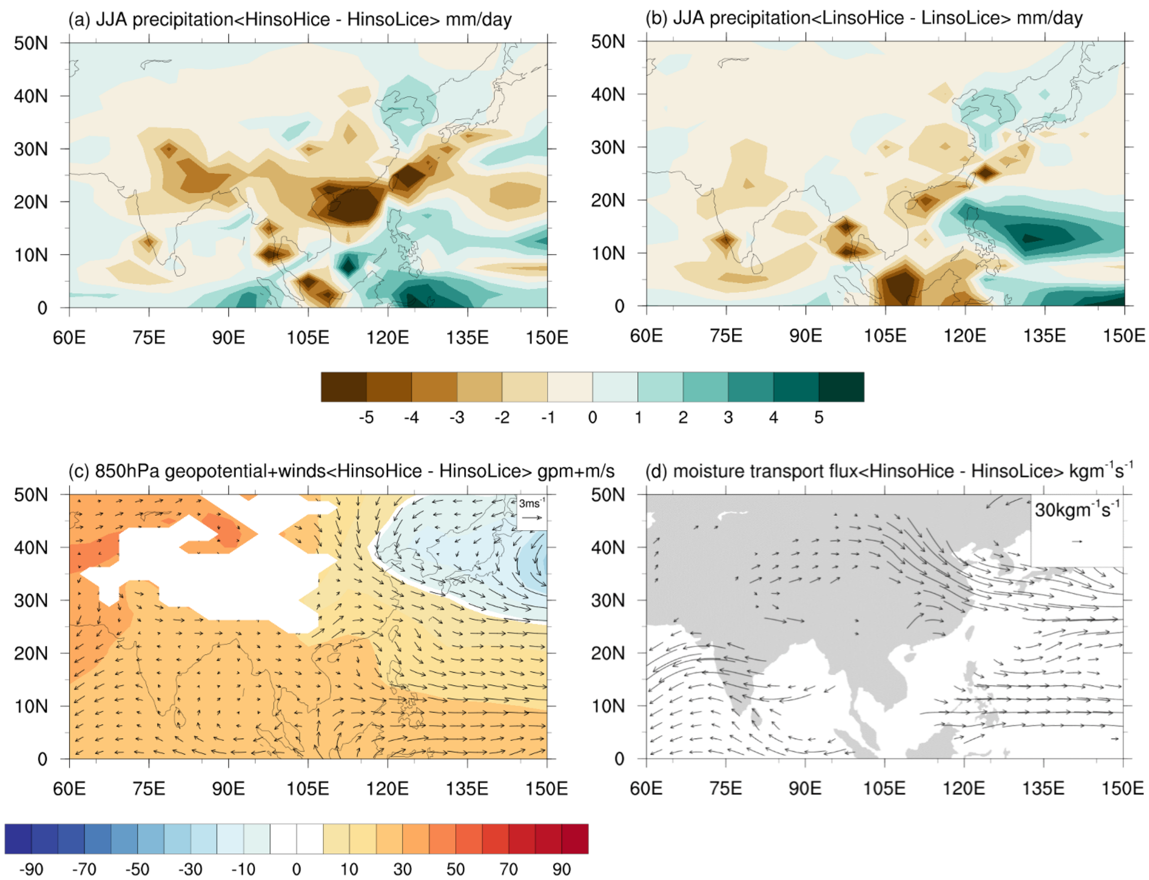
(a) JJA precipitation<HinsoHice - HinsoLice> mm/day
(b) JJA precipitation<LinsoHice - LinsoLice> mm/day
50N
40N
30N
20N
10N
0
60E
75E
90E
105E
120E
135E
150E
-5 -4 -3 -2 -1 0 1 2 3 4 5
(c) 850hPa geopotential+winds<HinsoHice - HinsoLice> gpm+m/s
3ms-1
(d) moisture transport flux<HinsoHice - HinsoLice> kgm-1s-1
30kgm-1s-1
-90 -70 -50 -30 -10 0 10 30 50 70 90

Figure 4

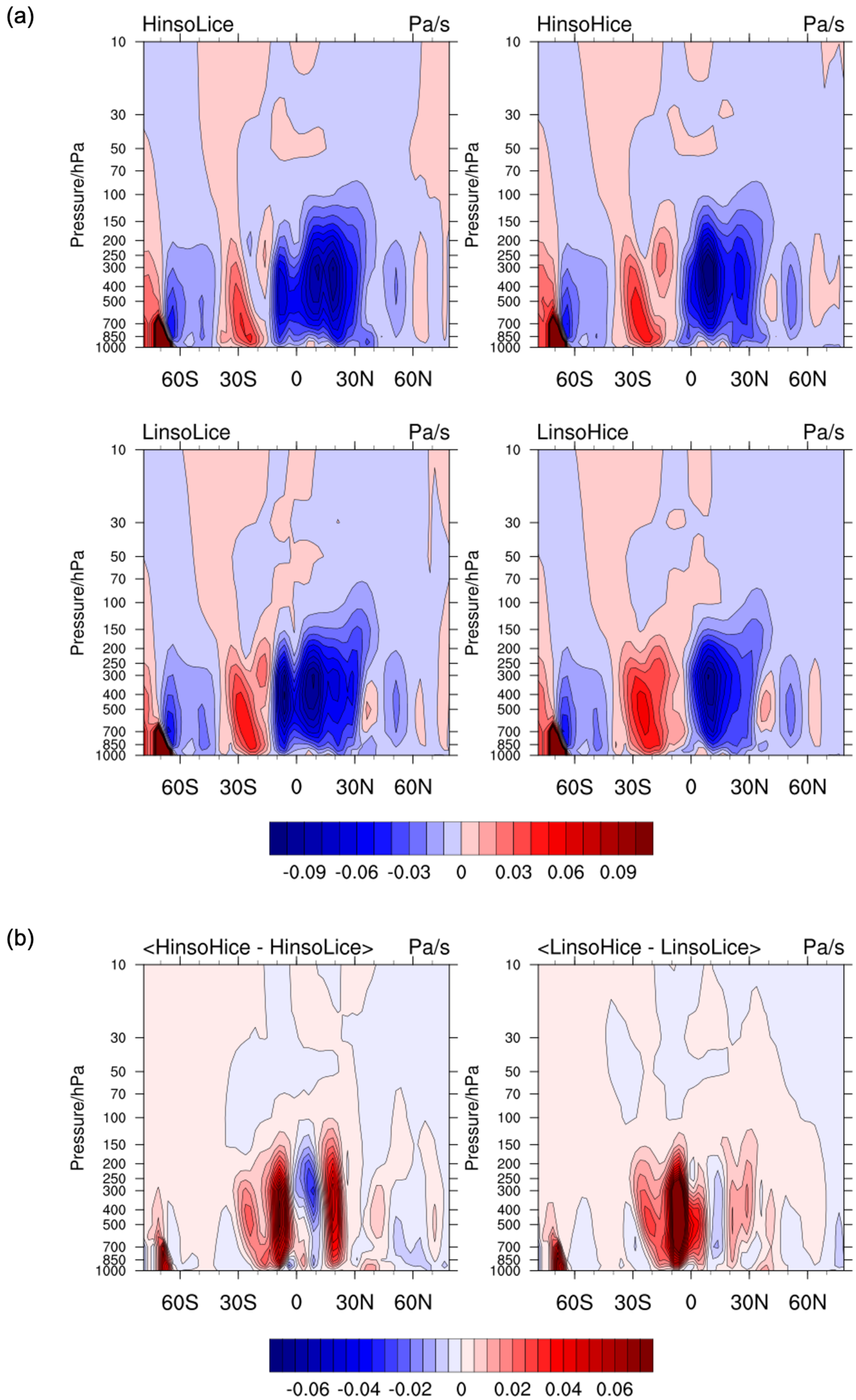
(a)
HinsoLice
Pa/s
HinsoHice
Pa/s
LinsoLice
Pa/s
LinsoHice
Pa/s
Pressure/hPa
10
30
50
70
100
150
200
250
300
400
500
700
850
1000
60S
30S
0
30N
60N
-0.09
-0.06
-0.03
0
0.03
0.06
0.09
(b)
<HinsoHice - HinsoLice>
Pa/s
<LinsoHice - LinsoLice>
Pa/s
-0.06
-0.04
-0.02
0
0.02
0.04
0.06